Rare processes in ultrahigh-energy tau-lepton transport

Guo-yuan Huang (黄国远)[1†]

[1]School of Mathematics and Physics, China University of Geosciences, 430074 Wuhan, China

Abstract: For cosmic neutrino observatories, charged-lepton transport is a key input for interpreting observables and reconstructing neutrino events. Charged leptons propagating through matter undergo several energy-loss processes, including electron-pair production and photonuclear interactions. In this work, we investigate several rare processes in tau-lepton transport, focusing primarily on muon pair production, $\tau N \to \tau\mu^+\mu^- N$, and Primakoff neutral-pion production, $\tau N \to \tau\pi^0 N$. At EeV energies, we find that the energy-loss contributions from muon pair production and Primakoff pion production are only 0.6% and 0.2%, respectively, of that from electron-pair production. Nevertheless, dimuon production may be relevant to tau-neutrino searches in underwater and under-ice Cherenkov telescopes. The interaction length for dimuon emission by an EeV tau is only 6 km in standard rock. Such events may be identified through the lateral separation of dimuon tracks or through a kebab topology if the tau decays in the detector. In addition, we emphasize that hard photonuclear scatterings during tau transport become increasingly important at the energy scales relevant for lunar neutrino searches such as SKA-Low.

Keywords: Ultrahigh-energy neutrinos, Charged-lepton transport, Neutrino telescopes

DOI: 10.1088/1674-1137/aeba75 **CSTR:**

CPC Accepted

I. INTRODUCTION

Over the past decades, IceCube observations have opened a new window into the high-energy universe and begun to shed light on the origins of ultrahigh-energy (UHE) neutrinos [1−9]. More recently, observations from KM3NeT have begun to extend our exploration of the neutrino flux toward the EeV energy frontier [10]. A central goal of next-generation UHE neutrino telescopes is to identify the astrophysical sources of these neutrinos and characterize the diffuse neutrino flux with greater precision [11−30]. Achieving this goal requires not only larger instrumented volumes but also a detailed understanding of how neutrinos and their secondary particles interact with matter.

UHE neutrinos are observed primarily through charged-current interactions, in which a neutrino converts into a charged lepton via W-boson exchange. Depending on the lepton flavor, the event may appear as a cascade or a track in underwater or under-ice detectors [13]. For neutrino telescopes that observe air showers (such as GRAND [19], POEMMA [25], BEACON [27], TAMBO [26], and similar experiments), the dominant signal is the decay of a tau lepton that emerges from a mountain or the ground after propagating tens of kilometers [31−43]. Even more ambitious proposals aim to detect UHE neutrinos (and cosmic rays) through the Moon, such as SKA-Low [44], by measuring the Askaryan radio signals generated by their interactions with the lunar regolith. A reliable description of charged-lepton propagation in matter is therefore essential for accurately reconstructing the energy and direction of the parent neutrino.

Charged-lepton transport is governed by several energy loss processes in matter, including bremsstrahlung, electron pair production, ionization, and photonuclear interactions [45−49]. These processes determine how far a charged lepton can travel from the interaction vertex. They also deposit energy along its trajectory, producing Cherenkov light that makes the track visible.

Above 100 TeV, the dominant energy loss channels in muon and tau transport are photonuclear interactions and electron pair production, $\ell N \to \ell e^+ e^- N$ [47], where ℓ denotes the charged lepton and N the nuclear target. At sufficiently high lepton energies, the required momentum transfer q from the nucleus in the t-channel photon exchange can be very small, such that the cross section can be significantly enhanced. Besides these leading channels, several rare processes in muon propagation have also been studied, including $\mu N \to \mu\mu^+\mu^- N$ [49−54] and

Received 28 August 2026; Accepted 28 October 2026

† E-mail: huangguoyuan@cug.edu.cn

Content from this work may be used under the terms of the Creative Commons Attribution 3.0 licence. Any further distribution of this work must maintain attribution to the author(s) and the title of the work, journal citation and DOI. Article funded by SCOAP[3] and published under licence by Chinese Physical Society and the Institute of High Energy Physics of the Chinese Academy of Sciences and the Institute of Modern Physics of the Chinese Academy of Sciences and IOP Publishing Ltd

$\mu N \to \mu\tau^+\tau^- N$ [55–60]. Their contributions to energy loss are small and can often be neglected in numerical simulations of lepton transport [49]. Nevertheless, they can produce distinctive signatures in underwater and under-ice neutrino telescopes [50, 51, 57, 58]. For example, muon pair production during muon transport can produce muon bundles [50, 51], whereas tau pair production can yield ditau-bang signatures [57, 58, 61]. The conversion of μ into ν_μ through weak interactions has also been considered as a rare process [49], but it can constitute a background to the lollipop signal in tau neutrino searches.

In this work, we focus on tau-lepton propagation, which has received less attention than muon propagation despite its growing importance. Tau transport is fundamental to tau neutrino detection and may also help underwater and under-ice telescopes isolate the tau-flavor component of the neutrino flux. Here, we mainly investigate two unexplored channels and discuss their possible implications for future tau neutrino searches: (i) muon pair production, $\tau N \to \tau\mu^+\mu^- N$, and (ii) Primakoff pion production, $\tau N \to \tau\pi^0 N$. The corresponding Feynman diagrams at tree level are shown in Fig. 1. Both processes become increasingly important as the tau energy increases. This behavior can be understood within the equivalent-photon approximation (EPA) [62, 63]. At very high lepton energies, collinear photon emission is enhanced, with a distribution that scales as $\rho_\gamma \sim \ln(E_\ell/m_\ell)$. The process may then be viewed as the conversion of this photon into a muon pair or a neutral pion in the electromagnetic field of the nucleus.

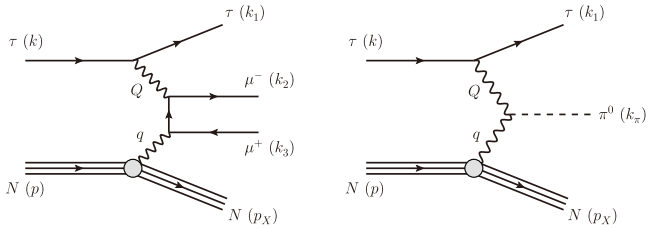

Fig. 1. Feynman diagrams for dimuon production (left) and Primakoff neutral-pion production (right) during tau-lepton propagation through matter. For dimuon production, an additional diagram with μ^+ and μ^- exchanged is not shown. Momenta are indicated along the diagram lines.

The remainder of this work is organized as follows. In Sec. II, we revisit the derivation of cross sections for dimuon and pion production and correct a coefficient in an expression in previous work. In Sec. III, we calculate the energy loss contributions of these processes and discuss their potential observable signatures. We also comment on the implications of $\tau \to \nu_\tau$ due to weak interactions. We conclude in Sec. IV.

II. CROSS SECTIONS

For the processes with two t-channel exchanges shown in Fig. 1, the cross section is dominated by the region of phase space characterized by small momentum transfers. In particular, the minimum momentum transfer scales approximately as $q^2_{\rm min} \approx m_\tau^2 m_V^2/E_\tau^2$ [45], where $m_V = 2m_\mu$ or m_π is the total mass of the produced state. For $E_\tau = 100\,\text{TeV}$, dimuon production has $q_{\rm min} \sim 3.7\,\text{keV}$, corresponding to a length scale comparable to the atomic size. At ultrahigh energies, the cross section is therefore dominated by inverse momentum transfers larger than the nuclear size, where the scattering receives a coherent Z^2 enhancement, but smaller than the atomic size, where screening becomes important.

In principle, calculating cross sections for pair production requires direct integration over the four-body final-state phase space [57]. Although the EPA and other approximations can simplify the cross-section calculation [64], deriving parameterized expressions based on these approximations is beyond the scope of this work. Moreover, the accuracy of the EPA depends on the photon virtuality, which must remain sufficiently small. We therefore directly integrate the $2 \to 4$ phase space for coherent nuclear scattering.

A. Cross section for muon pair production

The computational framework developed in Refs. [55–57] can be readily applied to muon pair production. We follow Ref. [57], which provides a detailed description and adopts a more modern convention. However, we identify a factor-of-four discrepancy in the cross-section formalism presented therein. To clarify the origin of this difference, we present the relevant derivation below, following the notation of Ref. [57] wherever possible, and compare the results at the points where they differ.

For muon pair production, the spin-averaged squared matrix element can be represented by

$$\frac{1}{4}\sum_{\rm spins}|\mathcal{M}|^2 = e^8 A_{\alpha\beta}\cdot B^{\alpha\beta}_{\mu\nu}\cdot 4\pi W^{\mu\nu}\cdot\frac{1}{t^2Y^2}\,, \tag{1}$$

where $t \equiv -q^2$ and $Y \equiv -Q^2$ are the momentum transfers associated with the nucleus and the charged lepton, respectively. The hadronic tensor is given by $W^{\mu\nu} = -g^{\mu\nu}F_1 + 2p^\mu p^\nu F_2/t$, where the structure functions F_1 and F_2 encode the nuclear form factor and atomic screening effect [57]. The tensor $A_{\alpha\beta} = 1/2\,\text{Tr}[(\not{k}_1 + m_\tau)\gamma_\alpha(\not{k} + m_\tau)\gamma_\beta]$ represents the contribution from the tau-lepton current, and $B^{\alpha\beta}_{\mu\nu}$ is the corresponding tensor for the lepton pair. The explicit expression for $B^{\alpha\beta}_{\mu\nu}$ is

CPC Accepted

$$B^{\alpha\beta}_{\mu\nu} = \mathrm{Tr}\Big[(\not{k}_2 + m_\mu) \Big(\gamma_\mu \frac{\not{k}_2 - \not{q} + m_\mu}{(k_2 - q)^2 - m_\mu^2} \gamma^\alpha + \gamma^\alpha \frac{\not{k}_2 - \not{Q} + m_\mu}{(k_2 - Q)^2 - m_\mu^2} \gamma_\mu \Big) (\not{k}_3 - m_\mu) \Big(\gamma_\nu \frac{\not{k}_2 - \not{Q} + m_\mu}{(k_2 - Q)^2 - m_\mu^2} \gamma^\beta + \gamma^\beta \frac{\not{k}_2 - \not{q} + m_\mu}{(k_2 - q)^2 - m_\mu^2} \gamma_\nu \Big) \Big], \quad (2)$$

where the contribution from the diagram with μ^+ and μ^- interchanged is also included.

The cross section can be expressed as

$$\mathrm{d}\sigma = \frac{\alpha^4}{\pi^4 \sqrt{\lambda_S}} \frac{A_{\alpha\beta} \cdot B^{\alpha\beta}_{\mu\nu} \cdot W^{\mu\nu}}{t^2 Y^2} \mathrm{d}\Phi_{\mathrm{PS}}, \quad (3)$$

where $\lambda_S \equiv (2p\cdot k)^2 - 4m_\tau^2 M_N^2$, and M_N denotes the target-nucleus mass. Because the original expression for the phase space is not explicitly given in Ref. [57], we specify our phase-space convention below:

$$\mathrm{d}\Phi_{\mathrm{PS}} = \mathrm{d}^4 q \frac{\mathrm{d}^3 k_1}{2E_1} \frac{\mathrm{d}^3 k_2}{2E_2} \frac{\mathrm{d}^3 k_3}{2E_3} \delta^4 (k + q - \sum_{i=1}^{3} k_i). \quad (4)$$

To carry out the integration, we transform to a set of variables appropriate for the two t-channel exchanges. Following Ref. [57], we introduce $(S_x, Y, M_x^2, t, V^2, \phi_1, \phi_q)$, with

$$S_x \equiv 2p\cdot Q, \quad Y \equiv -Q^2, \quad M_x^2 \equiv (p-q)^2, \quad t \equiv -q^2, \quad V^2 \equiv (q+Q)^2, \quad (5)$$

where ϕ_1 and ϕ_q are the azimuthal angles of $\boldsymbol{k}_1$ and $\boldsymbol{q}$, respectively; $\boldsymbol{k}$ ($\boldsymbol{Q}$) is chosen as the z axis in the rest frame of the target nucleus.

The first two differential factors, $\mathrm{d}^4 q\, \mathrm{d}^3 k_1$, in Eq. (4) can be expressed as

$$\frac{\mathrm{d}^3 \boldsymbol{k}_1}{2E_1} = \frac{1}{4\sqrt{\lambda_S}} \mathrm{d}S_x \mathrm{d}Y \mathrm{d}\phi_1, \quad (6)$$

$$\mathrm{d}^4 q = \frac{1}{4\sqrt{\lambda_Y}} \mathrm{d}M_x^2 \mathrm{d}t \mathrm{d}V^2 \mathrm{d}\phi_q, \quad (7)$$

where $\lambda_Y \equiv S_x^2 + 4M_N^2 Y$. In deriving these relations, we used the Jacobians

$$\frac{\partial(S_x, Y)}{\partial(|\boldsymbol{k}_1|, \cos\theta_1)} = \begin{vmatrix} -2M_t |\boldsymbol{k}_1|/E_1 & 0 \\ 2E_k |\boldsymbol{k}_1|/E_1 - 2|\boldsymbol{k}|\cos\theta & -2|\boldsymbol{k}||\boldsymbol{k}_1| \end{vmatrix} = \frac{2\sqrt{\lambda_S}|\boldsymbol{k}_1|^2}{E_1}, \quad (8)$$

$$\frac{\partial(M_x^2, t, V^2)}{\partial(E_q, |\boldsymbol{q}|, \cos\theta_q)} = \begin{vmatrix} -2M_t & -2|\boldsymbol{Q}| & 0 \\ 2E_q & -2|\boldsymbol{q}| & 0 \\ 2E_Q + 2E_q & 2|\boldsymbol{q}| - 2|\boldsymbol{Q}|\cos\theta & -2|\boldsymbol{q}||\boldsymbol{Q}| \end{vmatrix} = 4\sqrt{\lambda_Y}|\boldsymbol{q}|^2. \quad (9)$$

The phase space in Eq. (4) can be recast as

$$\mathrm{d}\Phi_{\mathrm{PS}} = \frac{1}{16\sqrt{\lambda_S \lambda_Y}} \mathrm{d}S_x \mathrm{d}Y \mathrm{d}\phi_1 \mathrm{d}M_x^2 \mathrm{d}t \mathrm{d}V^2 \mathrm{d}\phi_q \mathrm{d}\Phi_{\mathrm{pair}}, \quad (10)$$

which agrees with the final expression for the phase space used in the Appendix of Ref. [57]. Here, $\mathrm{d}\Phi_{\mathrm{pair}}$ denotes the phase space of the outgoing lepton pair,

$$\mathrm{d}\Phi_{\mathrm{pair}} = \frac{\mathrm{d}^3 k_2}{2E_2} \frac{\mathrm{d}^3 k_3}{2E_3} \delta^4 (k + q - \sum_{i=1}^{3} k_i) = \frac{1}{8} \sqrt{1 - \frac{4m_\mu^2}{V^2}} \mathrm{d}\cos\theta_\mu \mathrm{d}\phi_\mu, \quad (11)$$

where θ_μ and ϕ_μ are the zenith and azimuthal angles of $\boldsymbol{k}_2$ in the center-of-mass frame of the muon pair.

While the final expressions for the phase space agree, our differential cross section in Eq. (3) differs from Eq. (A1) of Ref. [57] by a factor of four. To determine whether this discrepancy is merely typographical, we attempt to reproduce the numerical result reported in that reference. We calculate the cross section for $\mu A \to \mu e^+ e^- X$ in standard rock, taking $Z = 11$ and $A = 22$. Figure 3 of Ref. [57] reports a total coherent-scattering cross section of $\sigma \approx 6.5 \times 10^{-25}\ \mathrm{cm}^2$ at $E_\mu = 10^8$ GeV. Our integration yields $\sigma \approx 6.45 \times 10^{-25}\ \mathrm{cm}^2$, in agreement with their result within the 0.1% numerical precision. Because Ref. [57] does not provide sufficient step-by-step details of the derivation, we cannot identify the exact point at which this prefactor mismatch arises. Nevertheless, our numerical results agree with those reported in Ref. [57], suggesting that the discrepancy is typographical rather than physical.

As a benchmark for tau transport, we calculate the cross section for $\tau N \to \tau \mu^+ \mu^- N$ in standard rock. At $E_\tau = 10^9$ GeV, we obtain $\sigma \approx 1.8 \times 10^{-29}\ \mathrm{cm}^2$. This is only 3×10^{-5} of the cross section for electron pair production by taus. However, as shown below, the corresponding contribution to energy loss is much larger than this cross-section ratio would suggest.

B. Cross section for Primakoff neutral-pion production

The calculation of the Primakoff process induced by charged leptons, $\tau N \to \tau \pi^0 N$, is similar to that for pair production. The framework developed in the previous subsection can be applied with minor modifications to the

CPC Accepted

matrix element and phase space.

The neutral pion couples to two photons through the axial anomaly. In the chiral limit, the amplitude for the $\pi\gamma\gamma$ coupling vertex is given by [65−67]

$$\Lambda_{\mu\nu}^{\pi^0\gamma\gamma}(q,Q) = \mathrm{i}\frac{\alpha}{\pi f_\pi}\epsilon_{\mu\nu\rho\sigma}q^\rho Q^\sigma\,, \tag{12}$$

where $f_\pi \approx 92\,\mathrm{MeV}$ denotes the pion decay constant, and E is the Levi-Civita symbol. Because the process is dominated by small momentum transfers, we use this low-energy amplitude without introducing a momentum-dependent form factor. The resulting matrix-element tensor is

$$B_{\mu\nu}^{\alpha\beta} = \epsilon_\mu^{\ \alpha\rho\sigma}\epsilon_\nu^{\ \beta\rho'\sigma'}q_\sigma Q_\rho q_{\sigma'}Q_{\rho'}\,. \tag{13}$$

The corresponding differential cross section is given by

$$\mathrm{d}\sigma = \frac{\alpha^4}{2\pi^5 f_\pi^2\sqrt{\lambda_S}}\frac{A_{\alpha\beta}\cdot B_{\mu\nu}^{\alpha\beta}\cdot W^{\mu\nu}}{t^2Y^2}\mathrm{d}\Phi_{\mathrm{PS}}\,. \tag{14}$$

The phase space is simpler than that for pair production and is given by

$$\begin{aligned}\mathrm{d}\Phi_{\mathrm{PS}} &= \mathrm{d}^4q\frac{\mathrm{d}^3k_1}{2E_1}\frac{\mathrm{d}^3k_\pi}{2E_\pi}\delta^4(k+q-k_1-k_\pi)\\ &= \frac{1}{16\sqrt{\lambda_S\lambda_Y}}\mathrm{d}S_x\mathrm{d}Y\mathrm{d}\phi_1\,\mathrm{d}M_x^2\mathrm{d}t\mathrm{d}\phi_q\,,\end{aligned} \tag{15}$$

where $V^2 = m_\pi^2$. The cross section is then obtained by integrating this expression.

III. OBSERVABLE EFFECTS

These new processes will contribute to tau energy loss, although they are expected to be subdominant relative to the standard channels. Nevertheless, quantifying their relative contributions is essential for a complete understanding of tau propagation. Furthermore, these subleading channels may produce distinctive observational signatures that could provide valuable probes of the underlying physics.

A. Energy loss contributions

If tau decay is neglected, the evolution of the tau energy in matter can be parameterized as $\mathrm{d}E/\mathrm{d}X = -\alpha - \beta E$, where α and β characterize the average energy-loss rate and depend only weakly on the energy E. The parameter α accounts for ionization, whereas β is dominated by contributions from pair production, bremsstrahlung, and photonuclear interactions. The parameter β is calculated as

$$\beta = \int \mathrm{d}y\, y\frac{\mathrm{d}\sigma}{\mathrm{d}y}\cdot\frac{N_{\mathrm{A}}}{A}\,, \tag{16}$$

where y is the fractional energy loss per collision, N_{A} is Avogadro's constant, and A is the mass number of the target atom.

Fig. 2 shows the energy loss parameter β as a function of the tau energy E_τ for several processes, with water/ice as the medium. The contributions from electron pair production (solid black curve) and bremsstrahlung (dotted black curve) approach their asymptotic values above $E_\tau = 10^6$ GeV. The red and yellow curves represent the contributions from muon-pair and Primakoff pion production, respectively. At $E_\tau = 10^9$ GeV, the muon-pair contribution is approximately 0.6% of the electron pair contribution, even though its cross section is only 0.003% as large. This difference arises because the cross section for electron pair production is dominated by the phase-space region with very small momentum transfers and, consequently, very small energy loss fractions y. Although the neutral-pion contribution continues to increase across the energy range shown in the plot, at $E_\tau = 10^9$ GeV it is only 0.2% of the electron pair contribution. Given the expected precision of future neutrino telescopes [11−30] and the uncertainties in the standard energy loss processes [47−49], these two channels can safely be neglected in lepton-transport simulations.

In Fig. 2, we also show the energy loss contribution from the conversion of τ into ν_τ through W-boson ex-

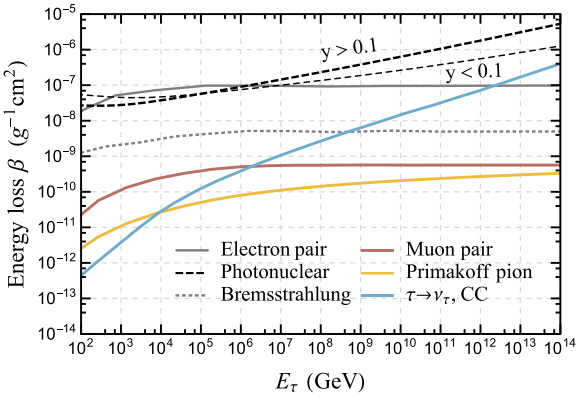

Fig. 2. (color online) The energy-loss parameter β is shown as a function of the tau energy E_τ. Muon pair production and Primakoff pion production are represented by the solid red and yellow curves, respectively. The standard contributions from electron pair production, photonuclear interactions (ALLM model), and bremsstrahlung are included for comparison [47]. We also show the energy loss associated with $\tau \to \nu_\tau$ induced by charged-current interactions [68], which has been considered a rare process for charged leptons in the literature. For the photonuclear interaction, we isolate contributions from different energy-loss fractions, namely $y > 0.1$ and $y < 0.1$.

CPC Accepted

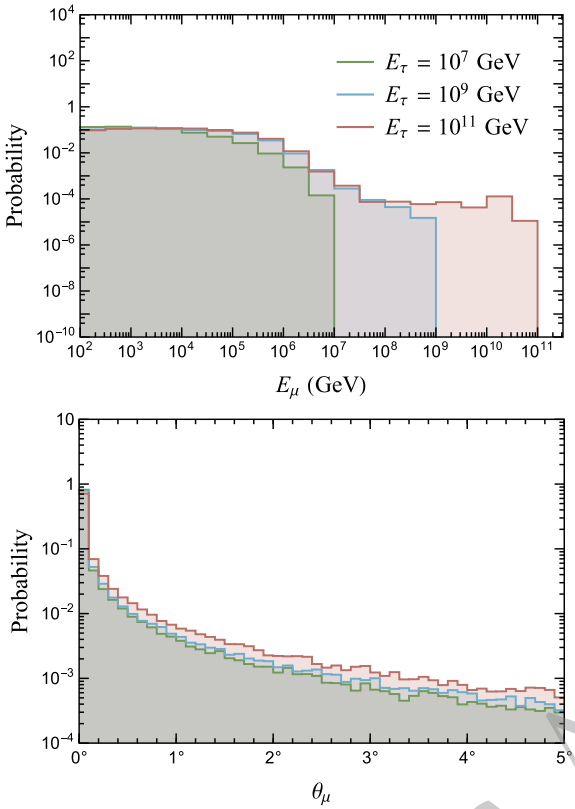

Fig. 3. (color online) Normalized distributions of the energies of the emitted muons (upper panel) and of the angle between a muon and the initial tau (lower panel). The initial tau energies are $E_\tau = 10^7$ GeV (green), 10^9 GeV (blue), and 10^{11} GeV (red).

change in weak interactions (blue curve). The weak energy loss is obtained with

$$\beta_{\rm weak} = \sigma_{\rm CC} N_A \,, \tag{17}$$

where the charged-current cross section $\sigma_{\rm CC}$ is taken from Ref. [68]. This process has traditionally been regarded as extremely rare and negligible compared with photonuclear interactions and pair production [49]. As shown in the figure, this assumption remains valid at lower tau energies. For $E_\tau \gtrsim 10^{10}$ GeV, charged-current scattering dominates the conversion of $\tau \to \nu_\tau$ over tau decay. For $E_\tau \gtrsim 10^{12}$ GeV (1 ZeV), the weak-interaction contribution exceeds that of electron pair production, although it remains smaller than that of photonuclear interactions (dashed black curves). We also note that, at 1 ZeV, energy loss due to photonuclear interactions is dominated by the hard component with inelasticity $y > 0.1$. Here, we discuss its implications for neutrino searches at ZeV energies.

Although most existing and proposed neutrino telescopes are not sensitive to ZeV neutrinos, this energy range is the primary target of lunar detection concepts for UHE cosmic neutrinos. Among these proposals, the SKA-Low telescope is expected to provide one of the most promising sensitivities [69]. SKA-Low aims to detect radio pulses generated by cascades induced by cosmic particles in the lunar regolith via the Askaryan effect. The coherent radio emission from these cascades can be measured by the low-frequency antenna array, enabling observations of neutrinos at energies far beyond the reach of conventional detectors.

SKA-Low is sensitive to all neutrino flavors. For ν_τ, however, previous sensitivity studies have typically discarded the produced tau lepton, assuming that only the initial interaction contributes to the radio signal [69, 70]. In this treatment, approximately 20% of the incident neutrino energy is deposited in the hadronic cascade at the interaction vertex, whereas the remaining 80%, carried away by the τ, has been neglected on the grounds that the τ undergoes only soft energy loss along its track. This approximation should break down when hadronic cascades from hard photonuclear interactions, i.e., $\tau N \to \tau X$ via photon exchange, are taken into account. During propagation, the secondary tau lepton can repeatedly initiate hadronic cascades through photonuclear interactions, producing Askaryan radio emission, as first noted in Ref. [71]. The contributions to energy loss from different inelasticity ranges are illustrated by the two dashed curves in Fig. 2, representing the soft component ($y < 0.1$) and the hard component ($y > 0.1$). The figure shows that hard energy losses become increasingly important at higher tau energies. At $E_\tau = 10^{14}$ GeV, photonuclear interactions with inelasticity $y > 0.1$ account for approximately 80% of the total energy loss. Consequently, each such interaction can deposit an energy comparable to that of the initial neutrino interaction vertex. Therefore, it is crucial to include these stochastic cascades induced by secondary taus in sensitivity estimates for lunar neutrino searches.

B. Dimuon signal from tau

Dimuon production during high-energy muon transport has been studied in previous works [50, 51] using simplified parameterizations of the cross section. Similar dimuon signatures can also arise from other Standard Model (SM) processes. A well-known source is charm production in charged-current deep inelastic scattering, $\nu_\mu + N \to \mu + {\rm c} + X$ followed by ${\rm c} \to {\rm s} + \mu + \nu_\mu$ [72–74]. Electroweak W-boson and trident production channels provide additional SM contributions [75–77]. Anomalous double-track signatures may also arise in new-physics scenarios involving heavy neutral leptons [78], secluded dark matter [79], leptogluons [80], supersymmetric particles [81, 82], boosted dark matter [83], among others. The typical signature of dimuon events consists of two tracks recorded simultaneously in the detector, provided that the lateral separation between the tracks is resolvable. Otherwise, they will be reconstructed as a

CPC Accepted

single track.

Similarly, dimuons can be produced along the trajectories of energetic tau leptons. We find that such production is common for an EeV tau lepton. For muon transport, identifying dimuons is challenging because the resulting dimuon system is highly boosted and embedded within the signal of the parent muon track. The tau lepton, however, provides a unique topology. In particular, a tau track can naturally produce a lollipop event when the tau decays inside the detector. In addition to laterally separated tracks, the accompanying high-energy dimuons continue to propagate beyond the tau-decay vertex, potentially giving rise to a distinctive signature. Below, we discuss the lateral separation and the potential new signature in turn.

1. *Lateral separation*

For track events in underwater or under-ice telescopes, the interaction vertex may lie either inside or outside the instrumented volume, corresponding to starting and through-going tracks, respectively. The dimuon track event has a distinctive topology, with two energetic muons correlated in time and direction. Because the two muons are strongly boosted along the direction of the incident particle, the identification of such events is fundamentally limited by the detector's ability to resolve their lateral separation, $D_{\mu\mu}$ [72]. In IceCube, the large instrumented volume is achieved using a sparse array of digital optical modules (DOMs). The horizontal (or vertical) separation between DOMs is approximately 125 m (or 17 m), which sets a lower limit on the resolvable lateral separation. Consequently, an approximate threshold of 34 m is typically required to effectively distinguish two parallel muon tracks [72, 73]. Because of this wide spacing, searches for dimuon events in IceCube are generally restricted. Future neutrino telescopes, such as KM3NeT [11], are expected to improve sensitivity to dimuons through denser detector configurations. Simulations indicate that arrays such as KM3NeT can resolve dimuon tracks with lateral separations down to the order of a few meters [73].

In the context of tau-lepton transport, we examine the kinematic properties of dimuons to assess whether the two produced tracks can be resolved through their lateral separation. The upper panel of Fig. 3 shows the normalized distribution of muon energy for initial tau energies $E_\tau = 10^7$ GeV, 10^9 GeV, and 10^{11} GeV. Fig. 4 illustrates that the pair energy is shared evenly between the two muons. Because the energy distributions of the two muons are symmetric, we do not distinguish between them. As shown in Fig. 3, an individual muon can carry an energy of the same order of magnitude as the initial tau, but the probability of such an event is only about 10^{-5}–10^{-4}. For $E_\tau = 1$ EeV, the average muon energy is about 1.3 TeV, which is well above the threshold of a typical water Cherenkov telescope.

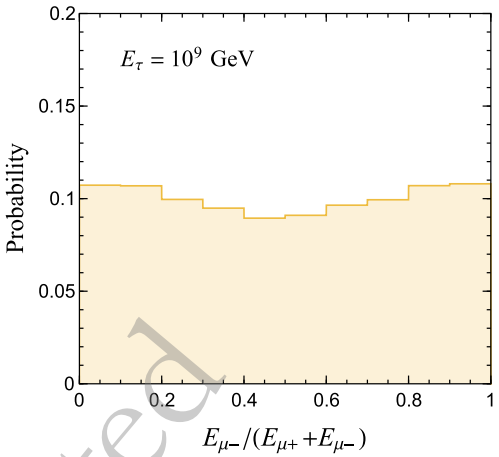

Fig. 4. (color online) The normalized distribution of the energy ratio defined as $E_{\mu^-}/(E_{\mu^+}+E_{\mu^-})$.

The two muons are also nearly collinear with the initial tau lepton. The lower panel of Fig. 3 shows the distribution of the angle θ_μ between the outgoing muon and the initial tau for several tau energies. The distribution depends only weakly on energy. At $E_\tau = 10^9$ GeV, the probability that this angle exceeds 0.1° (0.05°) is approximately 20% (30%). If the two muons are emitted with a nonzero opening angle, their separation increases as they propagate. For an angle θ_μ and propagation distance L, the characteristic lateral displacement is approximately $d_\perp \sim L\theta_\mu$. For a resolvable separation of 5 m and a propagation distance of O(5 km), the corresponding minimum angle is approximately O(0.06°).

If the two muon tracks overlap completely, geometric discrimination is no longer possible. In principle, they may still be distinguished statistically through their energy-loss patterns [84]. However, in practice, the stochastic nature of muon energy loss makes this discrimination approach very challenging.

2. *Kebab events*

In underwater and under-ice Cherenkov telescopes, the identification of tau neutrinos relies heavily on distinctive event topologies with low backgrounds, such as double bangs and lollipops [85, 86]. Although the classic double bang topology provides a relatively clean signature [87], it is constrained by the physical size of the detector. The tau decay length scales approximately as $L_\tau \approx 50\,\mathrm{m} \times (E_\tau/1\,\mathrm{PeV})$. At PeV energies, the decay length is on the order of tens of meters, allowing both cascades of a double bang to be resolved while remaining contained within a cubic-kilometer detector such as IceCube. However, as the energy approaches the EeV regime, L_τ increases to tens of kilometers, far exceeding the typical size of such instruments. In this case, an alternative signa-

CPC Accepted

ture is the lollipop topology [85, 88]. In a lollipop event, the initial ν_τ interaction occurs outside the instrumented volume. After kilometer-scale transport, the resulting tau track terminates in a hadronic or electromagnetic cascade inside the detector. Above 10 PeV, the lollipop topology significantly dominates the observable ν_τ event rate [85].

Dimuon production may be relevant for such lollipop events. To assess this, an important quantity is the number of dimuons produced along the tau trajectory. In Fig. 5, we show the interaction length, defined as the average distance a particle travels before undergoing a scattering event, as a function of tau energy. At $E_\tau = 10^9$ GeV, the tau travels an average distance of $L \approx 50$ km before decaying. In comparison, the relevant interaction length for dimuon emission is approximately $L \approx 6$ km in standard rock. This implies that an EeV tau will generate roughly $O(10)$ dimuon events during its propagation.

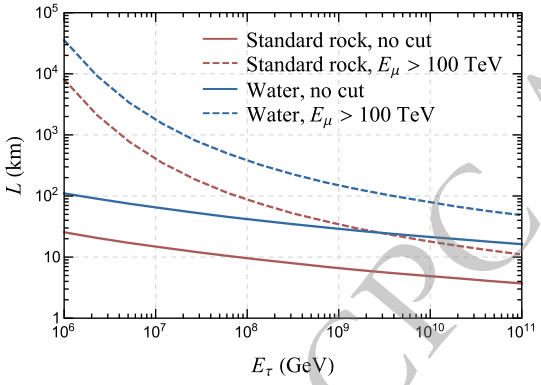

Fig. 5. (color online) The interaction length for muon pair production, defined as $L \equiv (\sigma n)^{-1}$, is shown as a function of the tau energy E_τ, where σ is the cross section and $n \equiv \rho N_A/A$ is the number density of target nuclei. The solid curves show the inclusive result, whereas the dashed curves correspond to the requirement that at least one muon has $E_\mu > 100$ TeV. Results are shown for standard rock (red) and water (blue).

An immediate consequence is that the lollipop topology may be accompanied by a muon pair. We can estimate the probability that these muons reach the detector in association with a lollipop event. Assuming a muon detection-energy threshold of 10 GeV and an energy cut at the production point of $E_0 = 100$ TeV, the maximum distance a muon can travel is determined by [51]:

$$E(X) = -\frac{\alpha}{\beta} + \left(\frac{\alpha}{\beta} + E_0\right) \mathrm{e}^{-\beta X}. \tag{18}$$

For muons propagating through standard rock, adopting $\alpha = 2.23 \times 10^{-3}$ GeV$\cdot$cm^2/g and $\beta = 4.64 \times 10^{-6}$ cm^2/g [47] yields a maximum propagation distance of $L \approx 4$ km. As shown in Fig. 5, the average interaction length required to produce a muon with an energy above 100 TeV is 40 km. Thus, approximately 10% of such lollipop events will be accompanied by dimuons if the EeV tau is produced at a distance of 4 km. For an initial tau energy of 10 EeV, this probability increases to 20% and would become even larger at higher neutrino energies.

The background of concern for such signals originates directly from tau-lepton decays. The muonic decay channel of the tau can produce an isolated high-energy muon (without an associated cascade) and generate a sugardaddy-like event [86, 89]. Such events should be distinguishable from lollipop events with dimuon tracks. However, the hadronic decay of the tau lepton (with a branching ratio of about 65%) in the detector can generate low-energy muons via secondary meson decays within the cascade. If both muons in the pair also have low energies, such pairs may be difficult to distinguish from the cascade muons. A quantitative assessment of this impact would require a detailed shower simulation.

IV. DISCUSSION

We have calculated the differential cross sections for rare processes during tau-lepton transport, including dimuon production and Primakoff neutral-pion production, and investigated their implications for UHE neutrino telescopes. At EeV energies, their contributions to tau energy loss are only 0.6% and 0.2%, respectively, of the contribution from electron–positron pair production. These processes can therefore be neglected in transport simulations at the precision expected for current and next-generation neutrino telescopes.

Despite their small contributions to energy loss, dimuons may produce distinctive signatures in underwater and under-ice Cherenkov detectors. At $E_\tau = 10^9$ GeV, approximately 20% of outgoing dimuon pairs are emitted at an angle greater than 0.1° relative to the initial tau direction, allowing the tracks to develop a potentially resolvable lateral separation. In addition, if the tau decays inside the detector, the companion muon pair can continue propagating through the detector, leaving tracks that extend beyond the tau decay vertex. The resulting topology resembles a kebab more closely than a traditional lollipop. We recognize that these dimuon events are very rare compared with the dominant experimental signals. Nevertheless, studying such events provides a complementary means of understanding neutrino interactions and the propagation behavior of their associated charged leptons.

ACKNOWLEDGMENTS

The author is indebted to Yong Du for many inspiring discussions and for his warm hospitality during the author's visit to the Institute of Modern Physics. The au-

CPC Accepted

thor also thanks Haoning He for stimulating discussions on the relevance of tau transport to SKA. The Feynman diagrams in Fig. 1 were generated using Jaxodraw [90]. This work is supported by the National SKA Program of China under Grant No. 2025SKA0110104 and by the "CUG Scholar" Scientific Research Funds at China University of Geosciences (Wuhan) under Project No. 2024014.

References

[1] IceCube, M. G. Aartsen *et al.*, Science **342**, 1242856 (2013), arXiv: 1311.5238

[2] IceCube, M. G. Aartsen *et al.*, Phys. Rev. Lett. **111**, 021103 (2013), arXiv: 1304.5356

[3] IceCube, M. G. Aartsen *et al.*, Science **361**(6398), 147 (2018), arXiv: 1807.08794

[4] IceCube, R. Abbasi *et al.*, Science **378**(6619), 538 (2022), arXiv: 2211.09972

[5] R. Abbasi *et al.*, "*Observation of high-energy neutrinos from the Galactic plane*," Science **380** (7, 2023) 6652, arXiv: 2307.04427.

[6] IceCube, R. Abbasi *et al.*, Science **380**(6652), adc9818 (2023), arXiv: 2307.04427

[7] IceCube, R. Abbasi *et al.*, Phys. Rev. Lett. **132**(15), 151001 (2024), arXiv: 2403.02516

[8] IceCube, R. Abbasi *et al.*, Phys. Rev. D **110**(2), 022001 (2024), arXiv: 2402.18026

[9] (IceCube Collaboration)§, IceCube, R. Abbasi *et al.*, Phys. Rev. Lett. **135**(3), 031001 (2025), arXiv: 2502.01963

[10] **KM3NeT**, S. Aiello *et al.*, "*Observation of an ultra-high-energy cosmic neutrino with KM3NeT*," Nature **638** (2025) no. 8050, 376–382.[Erratum: Nature 640, E3 (2025)].

[11] KM3Net, S. Adrian-Martinez *et al.*, J. Phys. G **43**(8), 084001 (2016), arXiv: 1601.07459

[12] TRIDENT, Z. P. Ye *et al.*, Nature Astron. **7**(12), 1497 (2023), arXiv: 2207.04519

[13] T.-Q. Huang, Z. Cao, M. Chen, J. Liu, Z. Wang, X. You, and Y. Qi, PoS **ICRC2023**, 1080 (2023)

[14] H. Zhang, Y. Cui, Y. Huang, S. Lin, Y. Liu, Z. Qiu, C. Shao, Y. Shi, C. Xie, and L. Yang, Astropart. Phys. **171**, 103123 (2025), arXiv: 2408.05122

[15] Baikal-GVD, V. A. Allakhverdyan *et al.*, Phys. Rev. D **107**(4), 042005 (2023), arXiv: 2211.09447

[16] IceCube-Gen2, M. G. Aartsen *et al.*, J. Phys. G **48**(6), 060501 (2021), arXiv: 2008.04323

[17] RNO-G, J. A. Aguilar *et al.*, JINST **16**(03), P03025 (2021), arXiv: 2010.12279

[18] A. Neronov, D. V. Semikoz, L. A. Anchordoqui, J. Adams, and A. V. Olinto, Phys. Rev. **D95**(2), 023004 (2017), arXiv: 1606.03629

[19] GRAND, J. Álvarez-Muñiz *et al.*, Sci. China Phys. Mech. Astron. **63**(1), 219501 (2020), arXiv: 1810.09994

[20] A. N. Otte, Phys. Rev. **D99**(8), 083012 (2019), arXiv: 1811.09287

[21] A. N. Otte, A. M. Brown, M. Doro, A. Falcone, J. Holder, E. Judd, P. Kaaret, M. Mariotti, K. Murase, and I. Taboada, "*Trinity: An Air-Shower Imaging Instrument to detect Ultrahigh Energy Neutrinos*," arXiv: 1907.08727.

[22] ARA, P. Allison *et al.*, Phys. Rev. D **102**(4), 043021 (2020), arXiv: 1912.00987

[23] Q. Abarr *et al.*, "*The Payload for Ultrahigh Energy Observations (PUEO): A White Paper*," arXiv: 2010.02892.

[24] A. Anker *et al.*, "*White Paper: ARIANNA-200 high energy neutrino telescope*," arXiv: 2004.09841.

[25] POEMMA, A. V. Olinto *et al.*, JCAP **06**, 007 (2021), arXiv: 2012.07945

[26] **TAMBO**, C. A. Argüelles *et al.*, "*TAMBO: A Deep-Valley Neutrino Observatory*," arXiv: 2507.08070.

[27] S. Wissel *et al.*, PoS **ICRC2019**, 1033 (2020)

[28] S. Wissel *et al.*, JCAP **11**, 065 (2020), arXiv: 2004.12718

[29] S. Ogawa and M. Sasaki, PoS **ICRC2021**, 970 (2021)

[30] K. de Vries *et al.*, PoS **ICRC2021**, 1195 (2021)

[31] V. S. Berezinsky and A. Y. Smirnov, Astrophys. Space Sci. **32**, 461 (1975)

[32] G. Domokos and S. Kovesi-Domokos, AIP Conf. Proc. **433**(1), 390 (1998), arXiv: hep-ph/9801362

[33] G. Domokos and S. Kovesi-Domokos, "*Observation of ultrahigh-energy neutrino interactions by orbiting detectors*," arXiv: hep-ph/9805221.

[34] K. S. Capelle, J. W. Cronin, G. Parente, and E. Zas, Astropart. Phys. **8**, 321 (1998), arXiv: astro-ph/9801313

[35] D. Fargion, A. Aiello, and R. Conversano, "*Horizontal tau air showers from mountains in deep valley: Traces of UHECR neutrino tau*," in *Proceedings, 26th International Cosmic Ray Conference (ICRC), August 17-25, 1999, Salt Lake City: Invited, Rapporteur, and Highlight Papers*, p. 396. 1999. arXiv: astro-ph/9906450. http://krusty.physics.utah.edu/icrc1999/root/vol2/h6_1_10.pdf.[2, 396(1999)].

[36] D. Fargion, Astrophys. J. **570**, 909 (2002), arXiv: astro-ph/0002453

[37] A. Letessier-Selvon, AIP Conf. Proc. **566**(1), 157 (2001), arXiv: astro-ph/0009444

[38] J. L. Feng, P. Fisher, F. Wilczek, and T. M. Yu, Phys. Rev. Lett. **88**, 161102 (2002), arXiv: hep-ph/0105067

[39] A. Kusenko and T. J. Weiler, Phys. Rev. Lett. **88**, 161101 (2002), arXiv: hep-ph/0106071

[40] X. Bertou, P. Billoir, O. Deligny, C. Lachaud, and A. Letessier-Selvon, Astropart. Phys. **17**, 183 (2002), arXiv: astro-ph/0104452

[41] Z. Cao, M. A. Huang, P. Sokolsky, and Y. Hu, J. Phys. **G31**, 571 (2005), arXiv: astro-ph/0411677

[42] E. Zas, New J. Phys. **7**, 130 (2005), arXiv: astro-ph/0504610

[43] B. Baret and V. Van Elewyck, Rept. Prog. Phys. **74**, 046902 (2011)

[44] T. Huege *et al.*, "*Measuring High-Energy Cosmic Particles with the SKA*," arXiv: 2606.28068.

[45] Y.-S. Tsai, "*Pair Production and Bremsstrahlung of Charged Leptons*," Rev. Mod. Phys. **46** (1974) 815.[Erratum: Rev.Mod.Phys. 49, 421–423 (1977)].

[46] I. A. Sokalski, E. V. Bugaev, and S. I. Klimushin, Phys. Rev. D **64**, 074015 (2001), arXiv: hep-ph/0010322

[47] J.-H. Koehne, K. Frantzen, M. Schmitz, T. Fuchs, W. Rhode, D. Chirkin, and J. B. Tjus, "*PROPOSAL: A tool for propagation of charged leptons*," Computer Physics Communications **184** (2013) no. 9, 2070–2090.

[48] I. Safa, J. Lazar, A. Pizzuto, O. Vasquez, C. A. Argüelles, and J. Vandenbroucke, Comput. Phys. Commun. **278**,

CPC Accepted

108422 (2022), arXiv: 2110.14662
[49] J.-M. Alameddine, J. Albrecht, H. Dembinski, P. Gutjahr, K.-H. Kampert, W. Rhode, M. Sackel, A. Sandrock, and J. Soedingrekso, Comput. Phys. Commun. **302**, 109243 (2024), arXiv: 2311.13357
[50] V. A. Kudryavtsev, E. V. Korolkova, and N. J. C. Spooner, Phys. Lett. B **471**, 251 (1999), arXiv: hep-ph/9911493
[51] S. R. Kelner, R. P. Kokoulin, and A. A. Petrukhin, Phys. Atom. Nucl. **63**, 1603 (2000)
[52] F. Maciuc *et al*., Phys. Rev. Lett. **96**, 021801 (2006)
[53] A. V. Berezhnoy, S. N. Koshkarev, and A. V. Luchinsky, "*Lepton pair production in muon scattering by nucleus*," arXiv: 0709.0422.
[54] G. Abbiendi, E. Budassi, C. M. Carloni Calame, A. Gurgone, and F. Piccinini, Phys. Lett. B **854**, 138720 (2024), arXiv: 2401.06077
[55] A. A. Akhundov, D. Y. Bardin, N. D. Gagunashvili, and N. M. Shumeiko, Sov. J. Nucl. Phys. **31**, 127 (1980)
[56] A. A. Akhundov, D. Y. Bardin, and N. M. Shumeiko, Sov. J. Nucl. Phys. **32**, 234 (1980)
[57] A. Bulmahn and M. H. Reno, Phys. Rev. D **79**, 053008 (2009), arXiv: 0812.5008
[58] A. P. Bulmahn, *Lepton pair production in high energy μA scattering: cross sections, energy loss, and applications to underground lepton production*. PhD thesis, Iowa U., 2010. https://inspirehep.net/files/fd079bce29b13f1202430c01271d9054.
[59] A. Bulmahn and M. H. Reno, Phys. Rev. D **82**, 057302 (2010), arXiv: 1007.4989
[60] S. Das, L. Kupari, M. H. Reno, and S. Trojanowski, "*Muon-induced di-tau production as a probe of new physics*," arXiv: 2606.05406.
[61] G.-y. Huang, Eur. Phys. J. C **82**(12), 1089 (2022), arXiv: 2207.02222
[62] C. F. von Weizsacker, Z. Phys. **88**, 612 (1934)
[63] E. J. Williams, Phys. Rev. **45**, 729 (1934)
[64] D. Ivanov, E. A. Kuraev, A. Schiller, and V. G. Serbo, Phys. Lett. B **442**, 453 (1998), arXiv: hep-ph/9807311
[65] C. D. Roberts, Nucl. Phys. A **605**, 475 (1996), arXiv: hep-ph/9408233
[66] M. R. Frank, K. L. Mitchell, C. D. Roberts, and P. C. Tandy, Phys. Lett. B **359**, 17 (1995), arXiv: hep-ph/9412219
[67] P. Maris and P. C. Tandy, Phys. Rev. C **65**, 045211 (2002), arXiv: nucl-th/0201017
[68] R. Gandhi, C. Quigg, M. H. Reno, and I. Sarcevic, Phys. Rev. D **58**, 093009 (1998), arXiv: hep-ph/9807264
[69] J. Bray *et al*., PoS **AASKA14**, 144 (2015)
[70] C. W. James and R. J. Protheroe, Astropart. Phys. **30**, 318 (2009), arXiv: 0802.3562
[71] D. García-Fernández, A. Nelles, and C. Glaser, Phys. Rev. D **102**(8), 083011 (2020), arXiv: 2003.13442
[72] B. Zhou and J. F. Beacom, Phys. Rev. D **105**(9), 093005 (2022), arXiv: 2110.02974
[73] C. Sun, F. Zhang, F. Hu, D. Xu, and J. Gao, Chin. Phys. C **47**(2), 023109 (2023), arXiv: 2201.03580
[74] C. Ternes, D. A. Fagundes, E. Huayra, and E. G. de Oliveira, JHEP **05**, 025 (2025), arXiv: 2412.12076
[75] S.-F. Ge, M. Lindner, and W. Rodejohann, Phys. Lett. B **772**, 164 (2017), arXiv: 1702.02617
[76] B. Zhou and J. F. Beacom, Phys. Rev. D **101**(3), 036010 (2020), arXiv: 1910.10720
[77] B. Zhou and J. F. Beacom, "*Neutrino-nucleus cross sections for W-boson and trident production*," arXiv: 1910.08090.
[78] P. Meade, S. Nussinov, M. Papucci, and T. Volansky, JHEP **06**, 029 (2010), arXiv: 0910.4160
[79] ANTARES, S. Adrián-Martínez *et al*., JCAP **05**, 016 (2016), arXiv: 1602.07000
[80] Y. Bai, K. Xie, and B. Zhou, "*Large Neutrino "Collider"*," arXiv: 2510.13948.
[81] I. Albuquerque, G. Burdman, and Z. Chacko, Phys. Rev. Lett. **92**, 221802 (2004), arXiv: hep-ph/0312197
[82] M. Ahlers, J. Kersten, and A. Ringwald, JCAP **07**, 005 (2006), arXiv: hep-ph/0604188
[83] P. S. B. Dev, B. Dutta, A. Karthikeyan, W. Maitra, L. E. Strigari, and A. Verma, "*'Dark' Matter Effect as a Novel Solution to the KM3-230213A Puzzle*," arXiv: 2505.22754.
[84] M. D. Kistler and R. Laha, Phys. Rev. Lett. **120**(24), 241105 (2018), arXiv: 1605.08781
[85] J. F. Beacom, N. F. Bell, D. Hooper, S. Pakvasa, and T. J. Weiler, "*Measuring Flavor Ratios of High-Energy Astrophysical Neutrinos*," Phys. Rev. D **68** (2003) 093005, arXiv: hep-ph/0307025.[Erratum: Phys.Rev.D 72, 019901 (2005)].
[86] IceCube, D. F. Cowen, J. Phys. Conf. Ser. **60**, 227 (2007)
[87] J. G. Learned and S. Pakvasa, Astropart. Phys. **3**, 267 (1995), arXiv: hep-ph/9405296
[88] IceCube, R. Abbasi *et al*., Phys. Rev. D **86**, 022005 (2012), arXiv: 1202.4564
[89] D. A. Fagundes, R. R. Francisco, and E. G. de Oliveira, Phys. Rev. D **100**(8), 083020 (2019), arXiv: 1903.05607
[90] D. Binosi, J. Collins, C. Kaufhold, and L. Theussl, Comput. Phys. Commun. **180**, 1709 (2009), arXiv: 0811.4113

CPC Accepted